Experimental study of a membrane-based liquid desiccant dehumidifier based on internal air temperature variation

Junze Chu[a], Jie Zhu[a,*], Hongyu Bai[a], Yuanlong Cui[b]

[a] Department of Architecture and Built Environment, the University of Nottingham

University Park, Nottingham, NG7 2RD, UK

[b] Department of Built Environment, College of Engineering and Technology, the University of Derby, Derby, DE22 3AW, UK

Abstract

A membrane-based liquid desiccant dehumidifier with the separated air stream and liquid desiccant channels has the ability to solve its working fluid carryover problem in the traditional direct contact system. The sensible, latent, total effectiveness and air moisture removal rate are adopted for the dehumidifier performance evaluation in this paper, and the dehumidifier main operating parameters are investigated experimentally to identify their influences and internal air temperature variations, including inlet air relative humidity (*RH*), inlet solution concentration and temperature, heat capacity rate ratio (*Cr**) and number of heat transfer units (*NTU*). It is found that both the inlet air *RH* and solution temperature have the negative influences on the dehumidifier effectiveness, while the desiccant solution concentration has little positive influence; the air moisture removal rate rises sharply with the inlet air *RH* and solution concentration. The highest sensible, latent and total effectiveness achieved in this study are 0.823, 0.802 and 0.810 respectively when both *Cr** and *NTU* are equal to 12. However the operating condition with *NTU*=8 and *Cr**=6 is recommended with the corresponding sensible, latent and total effectiveness of 0.758, 0.71 and 0.728 respectively.

Key words: Membrane based liquid desiccant dehumidifier; Temperature field; Performance evaluation; Experimental study.

*Corresponding author, E-mail address: jie.zhu@nottingham.ac.uk

Nomenclature

AC	Air conditioning
C	Concentration (kg/m^3)
$C_{air/sol}$	Heat capacity rate of air/solution (W/K)
c_p	Specific heat capacity ($J/(kg\ K)$)
*Cr**	Heat capacity ratio
d	Width of the channel (mm)
D_{AB}	Binary diffusion coefficient for water vapour in air (m^2/s)
D_h	Hydraulic diameter of the flow channel (mm)
h	Convective heat transfer coefficient ($W/(m^2\ K)$)
H	*LAMEE* height (mm)
*H**	Operating factor
ΔH	Enthalpy difference (J/kg)
k	Thermal conductivity ($W/(m\ K)$)
L	*LAMEE* length (mm)
LAMEE	Liquid to air membrane energy exchanger
LDAC	Liquid desiccant air conditioning
$\dot{m}_{air/sol}$	Mass flow rate (kg/s)
$\dot{m}_{rr}$	Air moisture removal rate (g/s)
NTU	Number of heat transfer units
p	Atmospheric pressure (Pa)
p_v	Water vapour partial pressure at the solution side (Pa)
RH	Relative humidity ($\%$)
T	Temperature ($^{\circ}C$)
U	Total heat transfer coefficient ($W/(m^2\ K)$)
W	Width of the *LAMEE* (mm)
$W_{air/sol}$	Humidity ratio (kg/kg)

Greek symbols

ε	Effectiveness

δ	Membrane thickness (mm)
ρ	Density (kg/m^3)
Subscripts	
air	Air flow
in	Inlet
lat	Latent
mem	Membrane
out	Outlet
sen	Sensible
sol	Solution flow
tot	Total

1. Introduction

Energy demands in recent years sharply increase with the population and improved comfort standard. About forty percent worldwide energy is consumed in building service aspect [1], and air conditioning (*AC*) is the main energy consumer in both domestic and commercial buildings [2]. Therefore, it is urgent to decrease the building *AC* energy consumption without compromising the human comfort [3]. Conventional vapour compression *AC* system overcools the process air with temperature lower than its dew point temperature then reheats it to the required temperature [4]. Therefore the conventional *AC* cooling process causes superfluous energy consumption and has low effectiveness in dealing with latent heat; moreover, the condensed water in the cooling tube could generate fungi, mould and bacteria [5].

As an alternative technology, liquid desiccant air conditioning (*LDAC*) system eliminates the above drawbacks of the conventional vapour compression *AC* system [6], and shows high energy efficiency in hot and humid climate. 26%-80% energy saving can be achieved in the *LDAC* system compared to the conventional system owing to its separated temperature and moisture treatments [7]. The *LDAC* system is more attractive than the solid desiccant *AC* system because of its low air pressure drop, low regeneration temperature and high moisture capture capacity [8]; it can utilize low grade heat (solar energy, waste heat) for regeneration and achieve energy storage by the liquid desiccant [9] as well as filter microorganism such as bacteria, mould and fungi etc. Furthermore, the *LDAC* system not only dehumidifies but also cools the process air simultaneously. Various aspects of the *LDAC* system have been

investigated. For instance, Wang et al. [10] conducted a research on the *LDAC* dynamic dehumidification process, and found that the packing thermal mass effects on the outlet air temperature and humidity are different. Luo et al. [11] studied the performance of a dynamic counter-current flow dehumidifier, and discovered that the film breakdown will significantly reduce the effective interfacial area at the low solution flow rate, and the liquid droplets in the air will occur at the high air flow rate, which will deteriorate the indoor air quality. Sreelal et al. [12] analyzed the structure data effects of a liquid desiccant dehumidifier and found that the air velocity should be set based on the channel geometric size for the optimal dehumidification performance. Experimental and numerical methods are also conducted in [13] [14] [15] to study the *LDAC* system performance.

Although the *LDAC* system has many advantages compared with the conventional *AC* system, the desiccant droplet carryover problem still exists in the direct contact type, which would cause corrosion and deteriorate indoor air quality [16]. The membrane-based *LDAC* system can eliminate the carryover thoroughly in which semi-permeable membranes are applied to separate the air stream and liquid desiccant solution. Only heat and water vapour are allowed to pass through the membranes. Therefore, the membrane-based *LDAC* becomes a popular research topic in recent years. Abdel-Salam et al. [17] explored the design parameter influence on a liquid to air membrane energy exchanger (*LAMEE*), their results demonstrate that both heat capacity rate ratio (*Cr**) and number of heat transfer units (*NTU*) have positive effects on the *LAMEE* performance, but the effects sharply reduce when their values over the critical points. Namvar et al. [18] investigated a *LAMEE* performance at both transient and steady states, and pointed out that the outdoor air condition has huge influence on the latent time constant while it has little influence on the sensible time constant; the operating factor has positive effect on the sensible effectiveness while it has negative influence on the latent effectiveness. Ge et al. [19] carried out a *LAMEE* performance study experimentally and numerically, and discovered that the latent effectiveness enhances with *NTU*, the moisture flux ratio reduces with *NTU* but increases with inlet solution concentration; both the moisture flux ratio and latent effectiveness increase with *Cr** but slightly decrease with inlet air temperature; Bai et al. [20] studied the parameter influence on a membrane-based liquid desiccant dehumidifier performance through experimental test, and found that the sensible effectiveness increases with *NTU*, the latent and total effectiveness enhance with the solution concentration. Moghaddam et al. [21] compared the performance of a small scaled *LAMEE* with that of a full scaled one, and demonstrated that the whole *LAMEE* performance can be predicted by a small

scaled one. Abdel- Salam et al. [22] investigated the air and solution flow maldistribution influences on the *LAMEE* performance, their results show that the main heat transfer resistance is in the air side for a flat plate *LAMEE*.

Other studies, such as the *LAMEE* solution-side effectiveness [23], completed membrane energy exchanger performance assessment and optimization [24], coupled heat and mass transfer in a *LAMEE* for field, aspect ratio and operation condition investigations [25], parallel-plate *LAMEE* performance with quasi-counter flow [26] and conjugate transport phenomena [27] [28], have been carried out. However, the above researches mainly focus on the terminal parameters (such as inlet and outlet air states), the *LAMEE* internal temperature fields are only simply mentioned by few numerical studies, and no experimental investigation has been carried out. The internal fields reflect the state change process, and should be clarified for the performance improvement. The aim of this paper is to study the main parameter effects on the *LAMEE* energy performance by observing its internal air temperature fields. The air temperature fields inside a cross flow *LAMEE* are clearly presented based on the experimental tests. The experimental results can be used for numerical modelling verification and performance optimization in the future, which fills the research gap to identify the internal air temperature variation in the *LAMEE*.

2. Experimental Facilities

2.1. Experimental apparatus

The experimental rig is illustrated in Fig.1, and the main components include a membrane based flat-plate regenerator, a membrane based flat-plate dehumidifier, a strong solution tank, a weak solution tank and three heat exchangers. The experimental rig is well thermally insulated to reduce the environment effect.

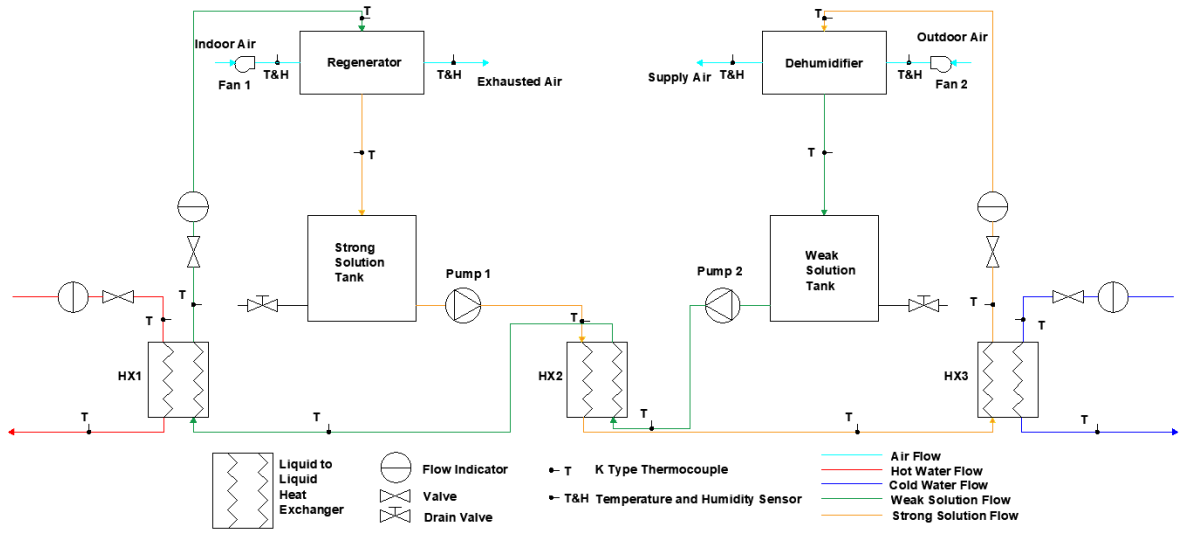

Fig. 1: Schematic diagram of the membrane based liquid desiccant *AC* system.

As indicated in Fig.1, the outdoor humid and hot fresh air flows into the dehumidifier, both its humidity ratio and temperature are reduced by the strong cold desiccant solution, the strong solution is diluted and becomes the weak solution. Afterwards the diluted solution is leaded to the weak solution tank, then pumped into a heat exchanger (HX2) for heat recovery. The weak solution is further heated in another heat exchanger (HX1) by hot water and then concentrated in the regenerator by the indoor exhaust air, afterwards it becomes the strong solution and is stored in the strong solution tank. Later the strong solution is pumped into HX2 for precooling, and then further cooled in the third heat exchanger (HX3) by cold water. Finally, the cooled concentrated desiccant solution flows into the dehumidifier for the next cycle. In the system, the strong and weak solutions are circulated by two 15W single phase magnetic driven pumps; two Parker UCC PET 1–15 L/min liquid flow meters are adopted to get the two solution flow rates.

2.2. Dehumidifier and sensors arrangement

The dehumidifier is shown in Fig.2 (a), its dimensions are 210*mm* (*H*) ×230*mm* (*W*) ×410*mm* (*L*). 22 air channels and 22 solution channels are formed in the dehumidifier, wavy line shape holders are adopted to support the air channels. The air flow is in the horizontal direction while the solution flow is in the vertical direction.

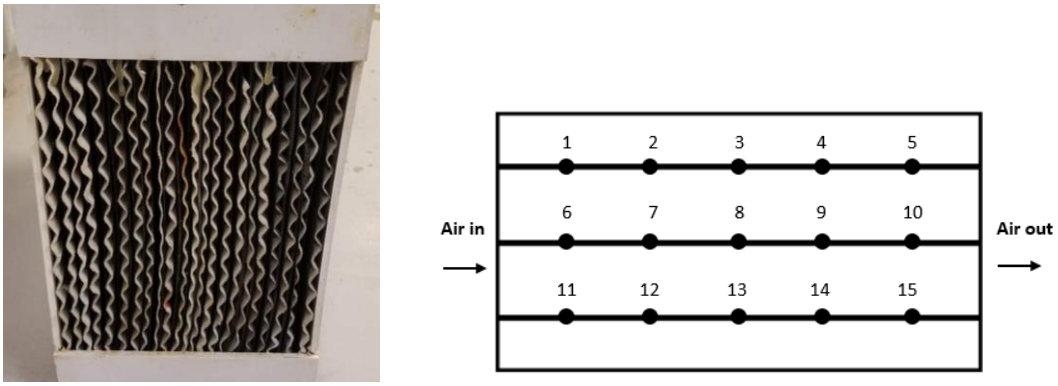

(a) (b)

Fig. 2: (a): Dehumidifier; (b): sensors arrangement in an air channel.

One air channel is selected for the air temperature measurement and 15 temperature sensors are installed as shown in Fig.2 (b). Three strips are placed with equal distance in the horizontal direction, and each strip holds 5 sensors. The *LAMEE* specifications and membrane properties are given in Table 1; the desiccant solution and air properties are listed in Table 2.

Table 1: Specifications of *LAMEE* and properties of membrane.

Parameter	Value
LAMEE length *L* (*mm*)	410
LAMEE Width *W* (*mm*)	230
LAMEE Height *H* (*mm*)	210
Width of air channel d_{air}(*mm*)	7.7
Width of solution channel d_{sol} (*mm*)	4.3
Membrane thickness δ(*mm*)	0.5
Membrane thermal conductivity k_{mem} (*W*/(*m K*))	0.3

Table 2: Properties of air and desiccant solution.

Parameter	Value
Specific heat capacity of air $C_{p,air}$ (*J*/(*kg K*))	1005
Specific heat capacity of desiccant solution $C_{p,sol}$ (*J*/(*kg K*))	2870
Air density ρ_{air} (kg/m^3)	1.17
Solution density ρ_{Sol} (kg/m^3)	1210
Air thermal conductivity k_{air} (*W*/(*m K*))	0.0264
Solution thermal conductivity k_{sol} (*W*/(*m K*))	0.53
Water vapour Binary diffusion coefficient in air D_{AB}(m^2/s)	2.25×10^{-5}

2.3. Measurement instruments

Testo 405i - Thermal anemometer is used to measure the air velocity; Sensirion Evaluation KIT EK-H4 sensors are adopted for the air temperature and relative humidity measurement, while K-type thermocouples are applied for the solution and water temperature measurement. Flow indicators and Parker Easiflow UCC are adopted to show the flow rates of water and the desiccant solution respectively. Brannan hydrometer is applied to get the desiccant solution density. Detailed instrument information is listed in Table 3.

Table 3: Measurement instrument capacities/calibration ranges and uncertainties.

Measurement instruments	Measurement range	Accuracy
Testo 405i - Thermal Anemometer Smart Probe	0-30m/s	±5%
Sensirion Evaluation KIT EK-H4	-40℃ to +125℃	±0.4%
	0-100%RH	±3%
K-type thermocouple probe Temperature	0-1100℃	±0.75%
RS Pro K type thermocouple glass fibre probe	-50℃ to+1000℃	±1.5%
DT500 Data logger	Data acquisition	±0.15%
Parker Easiflow UCC variable area flow meter	1-15L/min	±5%
Parker liquid flow indicator	2-22L/min	±2%
Brannan hydrometer	1-1.6g/ml	±2%

2.4. Uncertainly analysis

Uncertainly analysis is applied to calculate the uncertain range caused by the measurement instrument. A constant odds combination formula [29] is adopted.

$$\delta R = [(\frac{\partial R}{\partial x_1}\delta x_1)^2 + (\frac{\partial R}{\partial x_2}\delta x_2)^2 + \cdots (\frac{\partial R}{\partial x_N}\delta x_N)^2]^{\frac{1}{2}} \quad (1)$$

where R is the calculated value, $x_1, x_2 \ldots .x_N$ are the independent variables. The uncertainly analysis results are presented in results and discussion section.

3. Performance evaluation

The following operation and performance indexes are adopted in this study.

3.1. Operation index

The performance of a *LAMEE* is significantly affected by the operation factors which are listed as follows:

3.1.1. Operating factor H^*

Operating factor H^* is defined as the ratio of the latent energy difference to the sensible energy difference between the solution and air channels at the *LAMEE* inlets [30].

$$H^* = \frac{\Delta H_{Lat}}{\Delta H_{Sen}} \approx 2500 \frac{W_{air,in} - W_{sol,in}}{T_{air,in} - T_{sol,in}} \quad (2)$$

where $w_{air,in}$ is the inlet air humidity ratio (kg/kg), $w_{sol,in}$ is the equilibrium humidity ratio of the inlet solution (kg/kg), $T_{air,in}$ is the inlet air temperature ($℃$), and $T_{sol,in}$ is the inlet solution temperature ($℃$).

$w_{sol,in}$ can be calculated as [31]:

$$W_{sol,in} = 0.62198 \frac{P_v}{P - P_v} \quad (3)$$

where P_v is the water vapour pressure at the solution side of the membrane under equilibrium condition (Pa), which is given in [32]. P is the atmospheric pressure (Pa).

3.1.2. Heat capacity rate ratio Cr^*

Heat capacity rate ratio Cr^* is defined as the ratio of the liquid desiccant solution heat capacity rate to the air heat capacity rate:

$$Cr^* = \frac{C_{sol}}{C_{air}} = \frac{\dot{m}_{sol} C_{p,sol}}{\dot{m}_{air} C_{p,air}} \quad (4)$$

where C_{sol} is the solution heat capacity rate (W/K), C_{air} is the air heat capacity rate (W/K), $\dot{m}_{sol}$ is the solution mass flow rate (kg/s), $C_{p,sol}$ is the solution specific heat capacity ($J/(kg\ K)$), $\dot{m}_{air}$ is the air mass flow rate (kg/s), $C_{p,air}$ is the air specific heat capacity ($J/(kg\ K)$).

3.1.3. Number of heat transfer units NTU

Number of heat transfer units NTU is expressed as:

$$NTU = \frac{UA}{C_{min}} \quad (5)$$

$$U = \left[\frac{1}{h_{air}} + \frac{\delta}{k_{mem}} + \frac{1}{h_{sol}} \right]^{-1} \quad (6)$$

where U is the total heat transfer coefficient ($W/(m^2\ K)$), C_{min} is the minimum heat capacity rate between the desiccant solution and air (W/K), h_{air} is the air convective heat transfer coefficient ($W/(m^2\ K)$), k_{mem} is the membrane thermal conductivity ($W/(m\ K)$) and h_{sol} is the solution convective heat transfer coefficient ($W/(m^2\ K)$).

h_{air} and h_{sol} are obtained from the following equation in this study without considering the influence of water vapour mass transfer across the membrane:

$$Nu=\frac{hD_h}{k} \tag{7}$$

where h is the convective heat transfer coefficient of the fluid ($W/(m^2\ K)$); D_h is the hydraulic diameter of the flow channel (mm); k is the thermal conductivity of the fluid ($W/(m\ K)$).

Nu values for the air and solution are 6.58 and 8.06 respectively [33] [34] in this study.

3.2. Performance index

A most widely adopted performance index for energy exchanger is effectiveness [35]. In the study, the *LAMEE* performance is assessed by sensible, latent and total effectiveness. The sensible effectiveness is defined as the ratio of the actual sensible heat transfer rate to the maximum possible sensible heat transfer rate and expressed as:

$$\varepsilon_{sen}=\frac{T_{air,in}-T_{air,out}}{T_{air,in}-T_{sol,in}} \tag{8}$$

where $T_{air,out}$ is the air temperature at outlet ($℃$).

The latent effectiveness is defined as the ratio of the actual latent heat transfer rate to the maximum possible latent heat transfer rate, and given by:

$$\varepsilon_{lat}=\frac{W_{air,in}-W_{air,out}}{W_{air,in}-W_{sol,in}} \tag{9}$$

where $w_{air,out}$ is the outlet air humidity ratio (kg/kg).

The total effectiveness is defined as the ratio of the actual energy transfer rate to the maximum possible energy transfer rate, and presented by:

$$\varepsilon_{tot}=\frac{\varepsilon_{sen}+H^*\varepsilon_{lat}}{1+H^*} \tag{10}$$

Eqs (8) to (10) are meaningful only when the air capacity rate is lower than the solution capacity rate ($Cr^*\geq 1$).

Moisture removal rate is an important performance index for the *LAMEE*, and shows the moisture transfer rate between the air and solution channels.

$$\dot{m}_{rr}=\dot{m}_{air}|\ w_{air,out}\ -\ w_{air,in}| \tag{11}$$

where $\dot{m}_{rr}$ is the moisture removal rate (g/s).

4. Results and Discussion

The main parameters influencing the *LAMEE* performance are analysed, including Cr^*, NTU, inlet air humidity, inlet solution concentration and temperature. Table 4 lists the experiment

parameters for the inlet air and solution. Table 5 presents the experimental parameters for *NTU* and *Cr**.

Table 4: The experimental data for the inlet air and desiccant solution at *NTU*=*Cr**=8.

No.	Air *RH* (%)	No.	C_{sol}=30% T_{sol}(℃)	No.	C_{sol}=33% T_{sol}(℃)	No.	C_{sol}=36% T_{sol}(℃)	No.	C_{sol}=39% T_{sol}(℃)
1	62	**5**	18	**10**	18	**15**	18	**20**	18
2	66	**6**	20	**11**	20	**16**	20	**21**	20
3	70	**7**	22	**12**	22	**17**	22	**22**	22
4	74	**8**	24	**13**	24	**18**	24	**23**	24
		9	26	**14**	26	**19**	26	**24**	26

Table 5: The experimental data for *NTU* and *Cr** at T_{sol}=20℃, C_{sol}=33%, $T_{air,in}$=30℃ and *RH*=70%.

No.	*NTU*=4 *Cr**	No.	*NTU*=6 *Cr**	No.	*NTU*=8 *Cr**	No.	*NTU*=10 *Cr**	No.	*NTU=12 Cr**
1	2	**4**	2	**9**	2	**15**	2	**21**	2
2	4	**5**	4	**10**	4	**16**	4	**22**	4
3	6	**6**	6	**11**	6	**17**	6	**23**	6
		7	8	**12**	8	**18**	8	**24**	8
		8	10	**13**	10	**19**	10	**25**	10
				14	12	**20**	12	**26**	12

As shown in Tables 4 and 5, 48 experimental tests are conducted in this study. One set of air temperature distribution in the *LAMEE* is presented in Table 6 at *NTU*=8, *Cr**=6. The highest air temperature (32.83℃) is found at the position 11 (bottom-left corner of the *LAMEE*), which is even greater than the inlet air temperature (30.42℃). The reason is that the air in this area is heated by the latent heat in the absorption process from the liquid desiccant solution side. Relatively, the lowest air temperature area is noted at the top-right corner of the *LAMEE*.

Table 6: Air temperature field with *NTU*=8, *Cr**=6.

Air side (℃)					
Position	**1**	**2**	**3**	**4**	**5**
Temperature	28.73	27.93	27.11	25.11	23.93
Position	**6**	**7**	**8**	**9**	**10**
Temperature	30.11	28.93	28.13	26.87	25.44
Position	**11**	**12**	**13**	**14**	**15**
Temperature	32.83	30.73	29.53	28.14	26.84

4.1. Effects of solution property

The effects of the desiccant solution temperature and concentration on the *LAMEE* performance are displayed in Figs.3, 4 (a) and 5. It is obviously that the *LAMEE* effectiveness decrease with the desiccant solution temperature. For instance, when the inlet solution temperature increases from 18 ℃ to 26 ℃ with 30% concentration, the sensible, latent and total effectiveness reduce 0.052, 0.092 and 0.086 respectively, but the effectiveness reduce 0.074, 0.06 and 0.068 respectively with 39% solution concentration. The above results indicate the temperature of high concentrated desiccant solution has relatively obvious influence on the sensible effectiveness, while less influences on the latent and total effectiveness. This is because that the higher concentration solution enhances the dehumidification potential and effectiveness and results in more latent heat released, this latent heat further reduces the sensible effectiveness. High temperature solution increases its equilibrium surface vapour pressure and decreases the vapour pressure difference between the solution and air, so the dehumidification process becomes less effective. Similar tendency is also applied for the moisture removal rate variations with T_{SOL} under different C_{SOL} as indicated in Fig.4 (b). For example, the moisture removal rate decreases 31.29% (from 0.326g/s to 0.224g/s) when the solution temperature increases from 18℃ to 26℃ for 33% concentration solution.

With regard to the solution concentration effect, the sensible effectiveness reduces with the solution concentration, but the latent and total effectiveness increase. For example, when the solution concentration changes from 30% to 39%, the sensible effectiveness decrease 0.061 and 0.082 at the solution temperatures of 18℃ and 26℃ respectively, which demonstrates the solution concentration has more impact on the sensible effectiveness at the higher solution temperature; while the corresponding latent effectiveness increase 0.077 and 0.109 and the total effectiveness enhance 0.022 and 0.04 respectively. Therefore, using the high concentration solution at relatively high temperature is a feasible method to prominently improve the dehumidification performance. This is because the high concentration solution has low equilibrium surface vapour pressure which enhances the dehumidification ability. In the tested range, the highest total effectiveness of 0.78 is achieved when the solution concentration is 39% at 18℃, the lowest total effectiveness of 0.672 is reached when the solution concentration is 30% at 26℃. More obvious effects can be seen from Fig.4 (c), for example, when the solution concentration changes from 30% to 39%, the moisture removal rate increases 46.7% (from 0.257g/s to 0.377g/s) at the solution temperature of 20℃, furthermore, the moisture removal rate increases 58.96% (from 0.212g/s to 0.337g/s) at the solution temperature of 24℃.

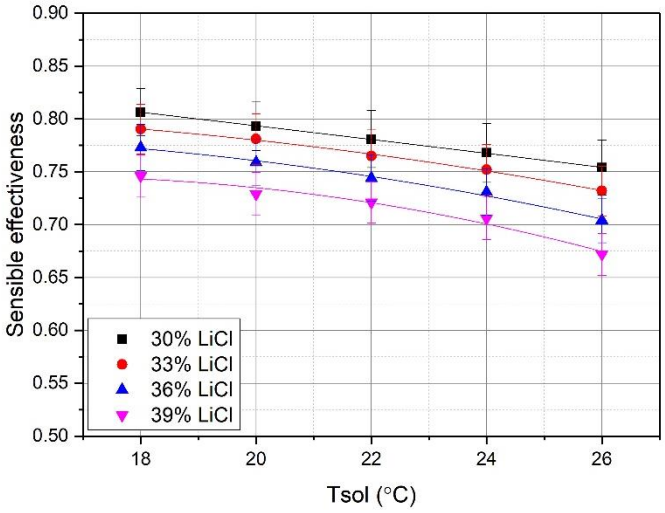

Fig. 3: Sensible effectiveness variations with T_{SOL} under different C_{SOL}.

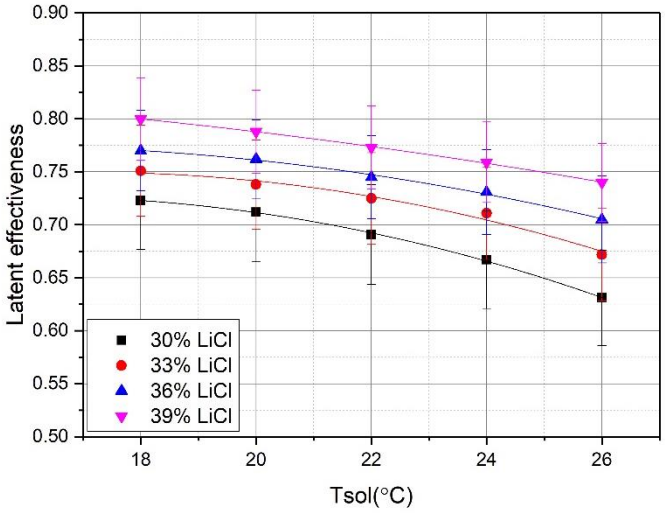

(a): Latent effectiveness variations with T_{SOL} under different C_{SOL}.

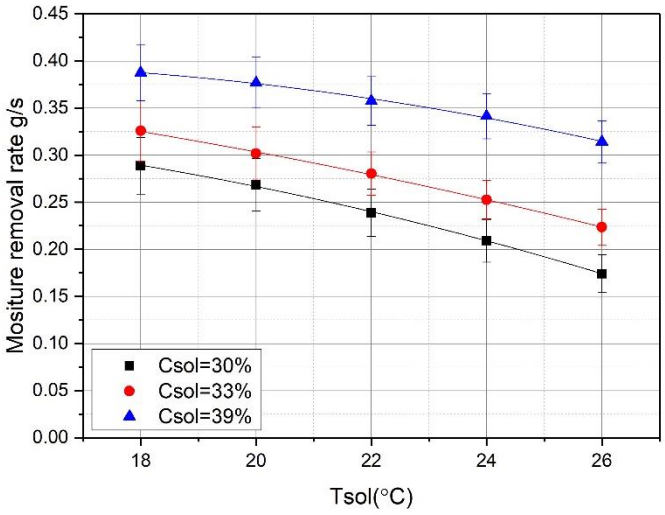

(b): Moisture removal rate variations with T_{SOL} under different C_{SOL}.

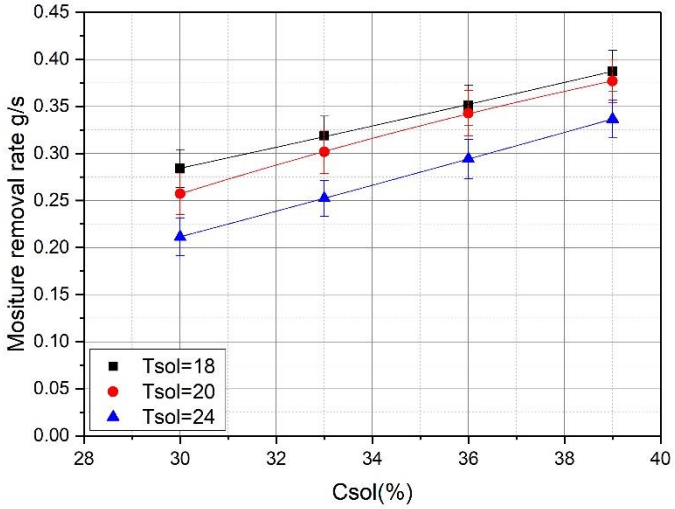

(c): Moisture removal rate variations with C_{SOL} under different T_{SOL}.

Fig. 4: Effects of solution property on latent effectiveness and moisture removal rate.

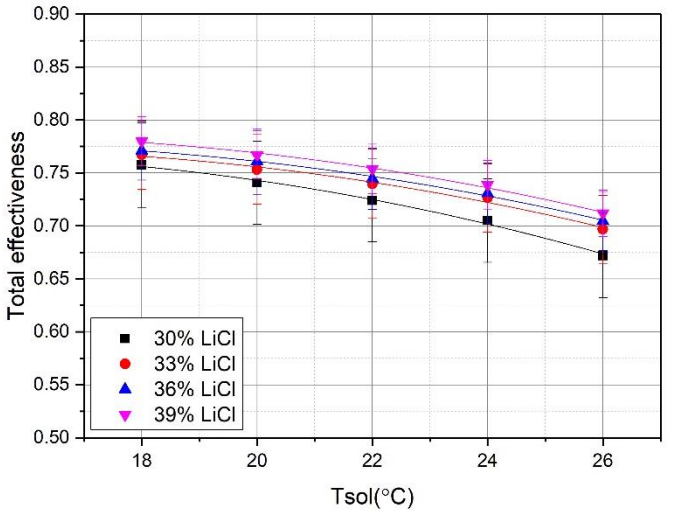

Fig. 5: Total effectiveness variations with T_{SOL} under different C_{SOL}.

4.2. Effects of inlet air relative humidity

The inlet air *RH* influences on the sensible, latent and total effectiveness are given in Fig.6 (a). It is found that the *LAMEE* effectiveness are rarely affected by the inlet air *RH*. When the air *RH* changes from 62% to 76%, the sensible and total effectiveness decrease from 0.829 to 0.768, and from 0.763 to 0.746 respectively, while the latent effectiveness increases from 0.716 to 0.734, this is because that the high relative humidity results in more moisture to be absorbed

by the solution, then the corresponding more latent heat is released to increase the air temperature. However, increasing the air relative humidity can dramatically improve the moisture removal rate as indicated in Fig.6 (b). When the air *RH* changes from 62% to 74%, its moisture removal rate rises 32.7% (from 0.245*g*/*s* to 0.325*g*/*s*). Therefore the proper performance index should be considered to evaluate the *LAMEE* performance.

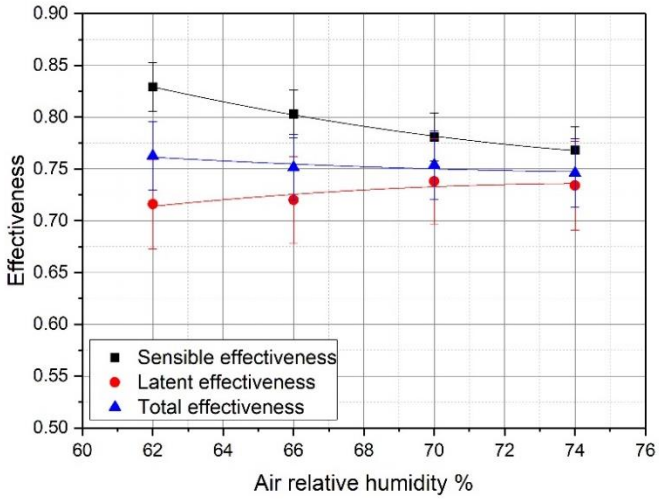

(a): Sensible, latent and total effectiveness variations with inlet air *RH*.

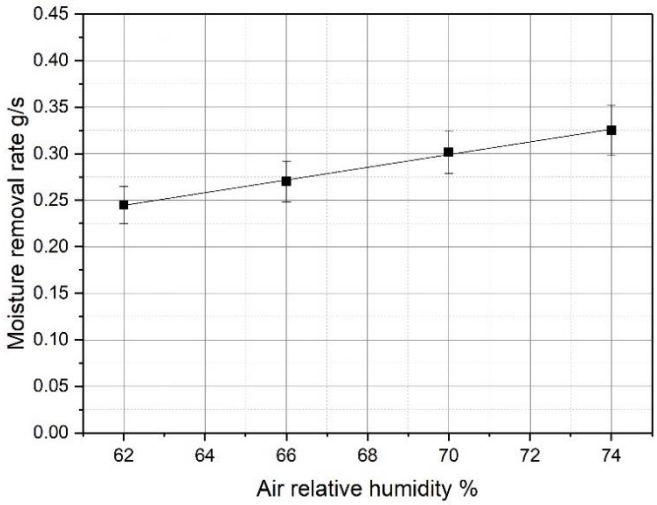

(b): Air relative humidity influence on the moisture removal rate.

Fig. 6: Effects of inlet air *RH* on effectiveness and moisture removal rate.

4.3. Effects of *Cr**

The air temperature variations with *Cr** in the *LAMEE* at *NTU*=8 are shown in Figs.7, 8 and 9. It can be seen that the temperature variation tendencies are similar for different *Cr**, but the high temperature location is different. The high temperature area moves towards the left side

with *Cr**. Overall, the highest air temperature is at the corner of the solution outlet and air inlet, and the lowest temperature is at the corner of the solution inlet and air outlet. The high temperature area reduces with *Cr**, and the temperature variation becomes smooth.

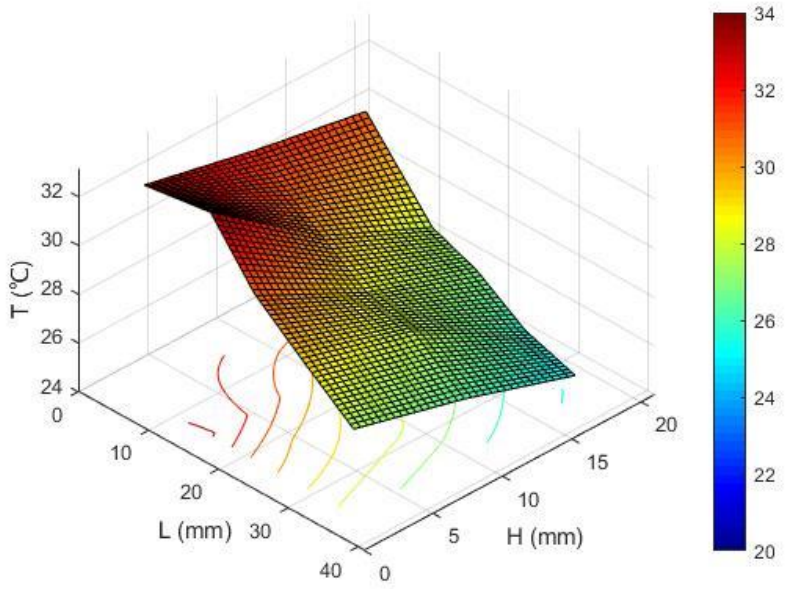

Fig. 7: Air temperature field when *Cr**=2, *NTU*=8.

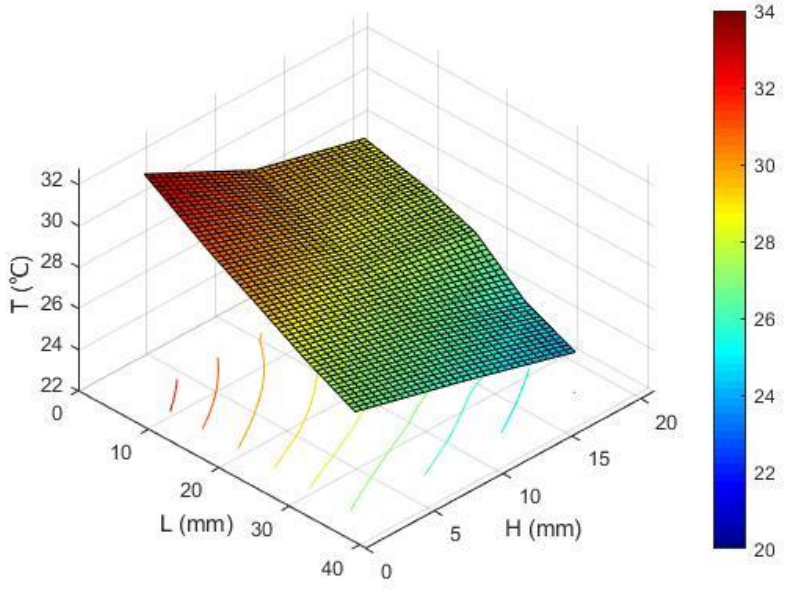

Fig. 8: Air temperature filed when *Cr**=6, *NTU*=8.

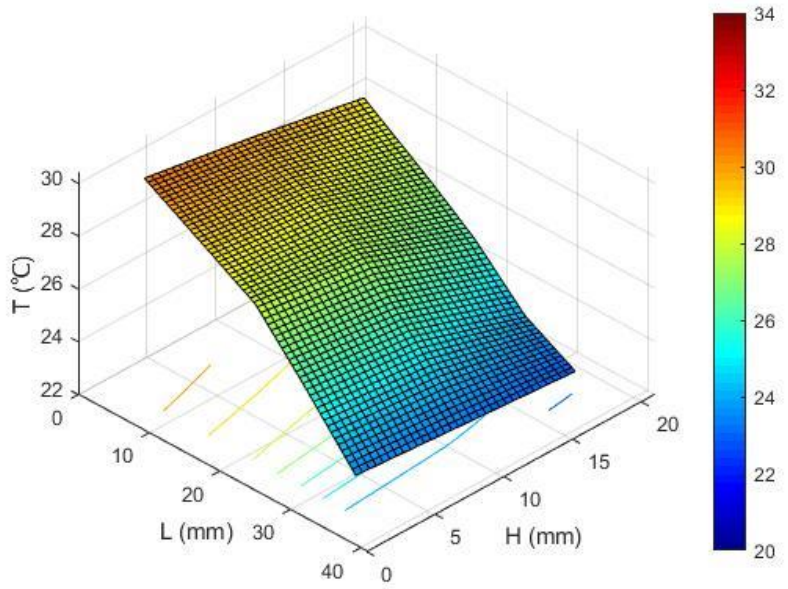

Fig. 9: Air temperature filed when *Cr**=10, *NTU*=8.

The influence of *Cr** on the *LAMEE* effectiveness under different *NTU* values are given in Figs.10, 11(a) and 12. The moisture removal rate variations with *Cr** under different *NTU* is indicated in Fig.11 (b). It is obvious that *Cr** has significant positive influences on the *LAMEE* effectiveness and moisture removal rate. For instance, at *NTU*=8, the sensible, latent and total effectiveness increase 0.299, 0.291 and 0.293 respectively as *Cr** changes from 2 to 12, and the moisture removal rate improves 71.58% (from 0.183*g*/*s* to 0.314*g*/*s*). However, the increase gradients dramatically decrease when *Cr** is greater than 6. Taking *NTU*=8 as an example, when *Cr** rises from 2 to 6, the sensible, latent and total effectiveness increase 0.258, 0.233 and 0.241 respectively; while the corresponding effectiveness only increase 0.033, 0.04 and 0.039 respectively when *Cr** changes from 6 to 10. The same situation is applied for the moisture removal rate, such as at *NTU*=8, the moisture removal rate improves 58.47% (from 0.183*g*/*s* to 0.290*g*/*s*) when *Cr** rises from 2 to 6, but it only increases 5.86% (from 0.290*g*/*s* to 0.307*g*/*s*) when *Cr** changes from 6 to 10. According to Eq (4), the high *Cr** means the high solution flow rate or short contact time between the air and desiccant solution, which leads to the high vapour pressure difference between them, the low solution temperature and high solution concentration. Moreover, the low *Cr** limits *NTU* effects on the *LAMEE* effectiveness. For instance, when *Cr**=2, the sensible, latent and total effectiveness increase only 0.147, 0.17 and 0.161 respectively as *NTU* varies from 4 to 12, but for *Cr**=6, the corresponding effectiveness increase 0.19, 0.199 and 0.196 respectively. In this study, the highest sensible, latent and total effectiveness reach 0.823, 0.802 and 0.810 respectively as *Cr**=*NTU*=12, and

the lowest effectiveness are 0.378, 0.34 and 0.356 respectively as *Cr**=2 and *NTU*=4. But considering the effectiveness increase gradient and its value, the recommend operation parameters are *Cr**=6, *NTU*=8 and the corresponding effectiveness are 0.758, 0.71 and 0.728 respectively.

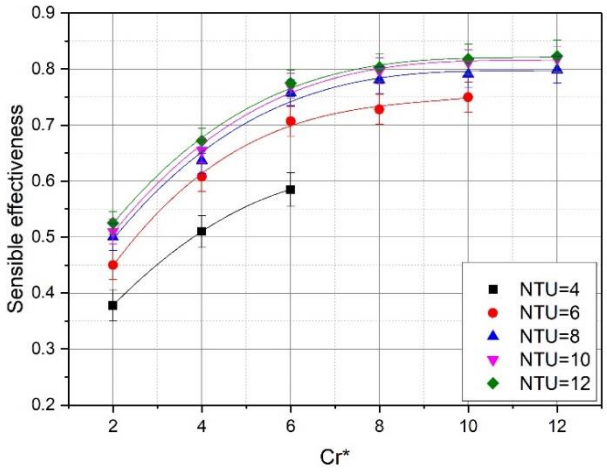

Fig. 10: *Cr** influence on sensible effectiveness under different *NTU*.

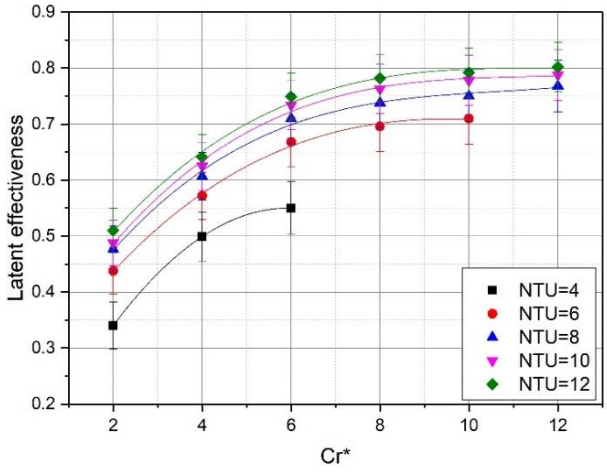

(a): *Cr** influence on latent effectiveness under different *NTU*.

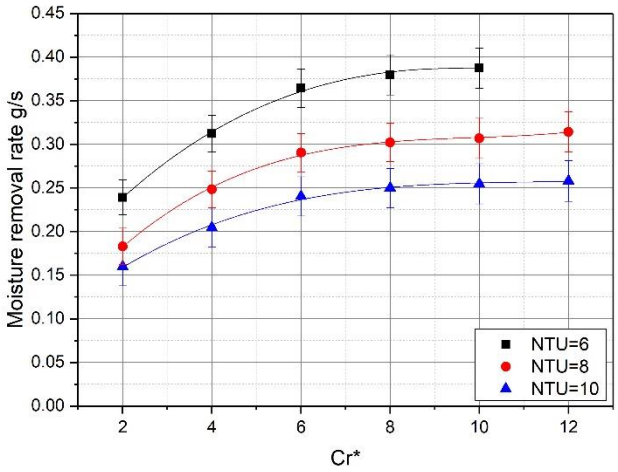

(b): Moisture removal rate variations with *Cr** under different *NTU*.

Fig. 11: *Cr** effects on latent effectiveness and moisture removal rate.

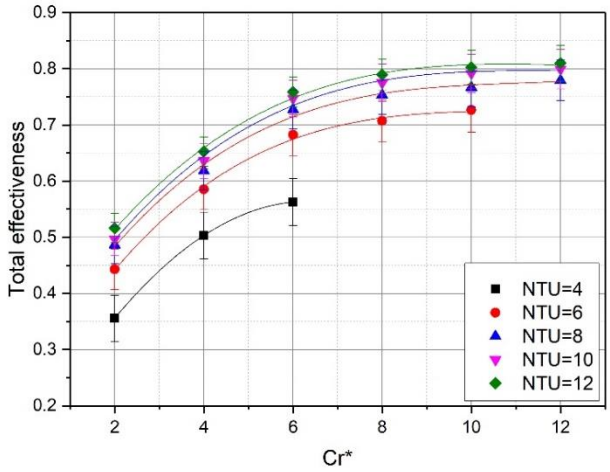

Fig. 12: *Cr** influence on total effectiveness under different *NTU*.

4.4. Effects of *NTU*

The air temperature variations with *NTU* are shown in Figs.13 and 14. Both the high and low temperature areas become small when *NTU* is low. This is due to the fact that the low *NTU* means the high air flow rate which reduces the contact time between the air and desiccant solution. The highest and lowest temperatures for *NTU*=4 and *NTU*=12 are 29.98℃ and 22.88℃, 33.01℃ and 20.99℃ respectively. The high *NTU* value stimulates the latent heat release at the corner of the solution outlet and air inlet, and increases the *LAMEE* effectiveness.

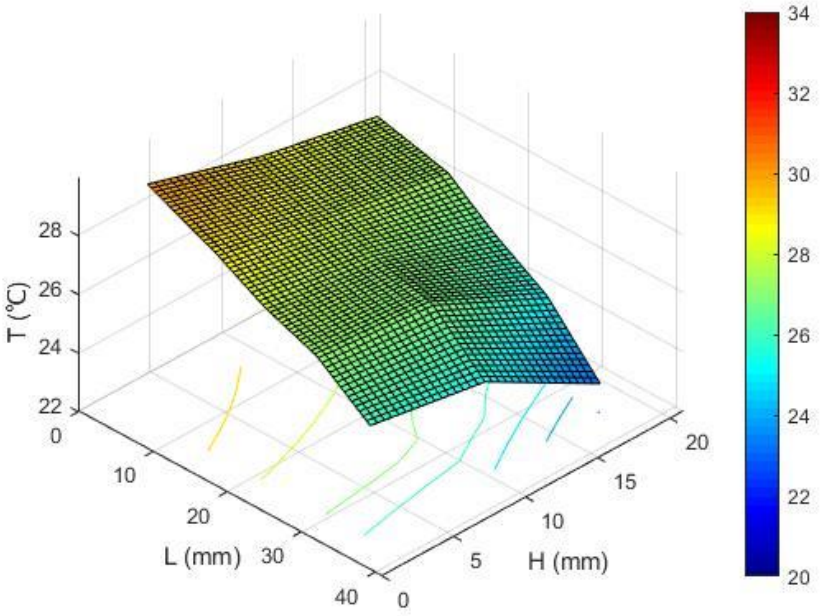

Fig. 13: Air temperature field when *Cr**=6 *NTU*=4.

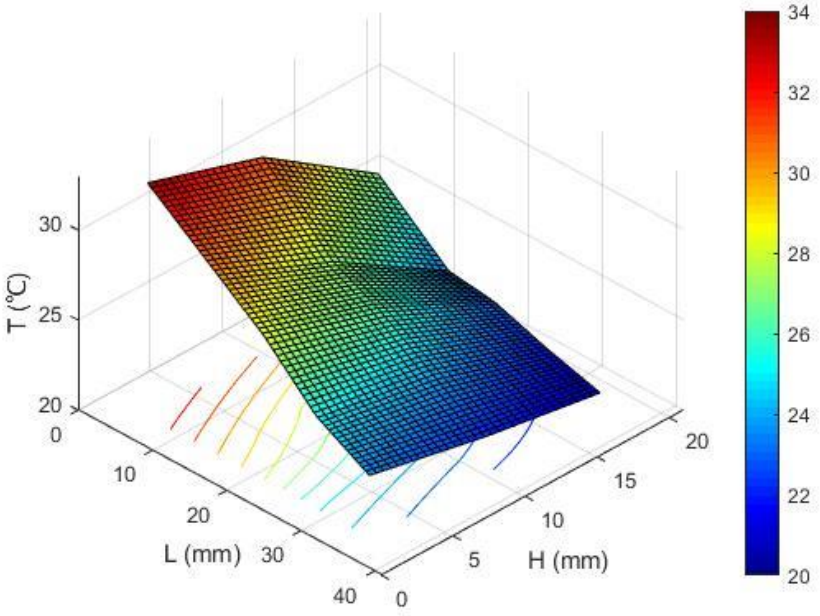

Fig. 14: Air temperature field when *Cr**=6 *NTU*=12.

The influences of *NTU* on the *LAMEE* effectiveness under different *Cr** values are plotted in Figs.15, 16 (a) and 17. Similar to the *Cr** effects, the *LAMEE* effectiveness increase with *NTU*. For instance, when *Cr**=6, the sensible, latent and total effectiveness increase 0.19, 0.199 and 0.196 respectively as *NTU* changes from 4 to 12. The effectiveness increase gradients sharply

decrease when *NTU* is greater than 8. Taking *Cr**=6 as an example, the sensible, latent and total effectiveness increase 0.173, 0.16 and 0.165 respectively as *NTU* changes from 4 to 8, while these effectiveness only increase 0.017, 0.039 and 0.031 as *NTU* varies from 8 to 12. According to Eq (5), the high *NTU* value means the low air flow rate, the low air flow rate extends the contact time between the air and desiccant solution, hence improves the *LAMEE* performance. Therefore *NTU*=8 is suggested for the tested system by considering both of the effectiveness increasing gradient and its value. However, *NTU* has the negative influence on the moisture removal rate, for example, at *Cr**=8, the moisture removal rate decreases 43.95% (from 0.380*g*/*s* to 0.213*g*/*s*) when *NTU* increases from 6 to12 as shown in Fig.16 (b).

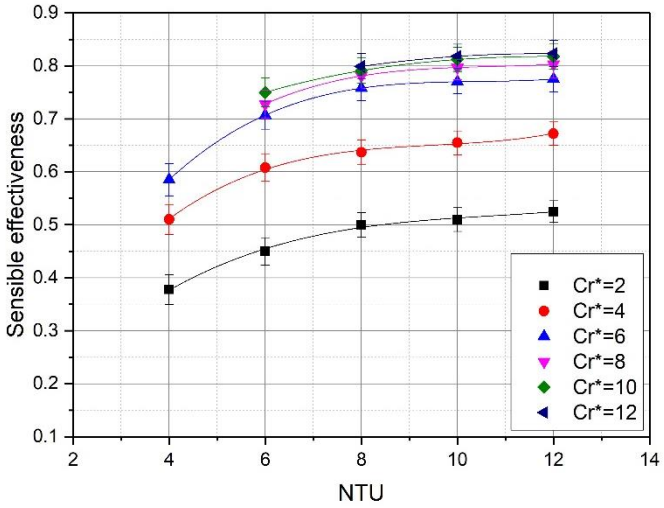

Fig. 15: *NTU* influence on sensible effectiveness under different *Cr**.

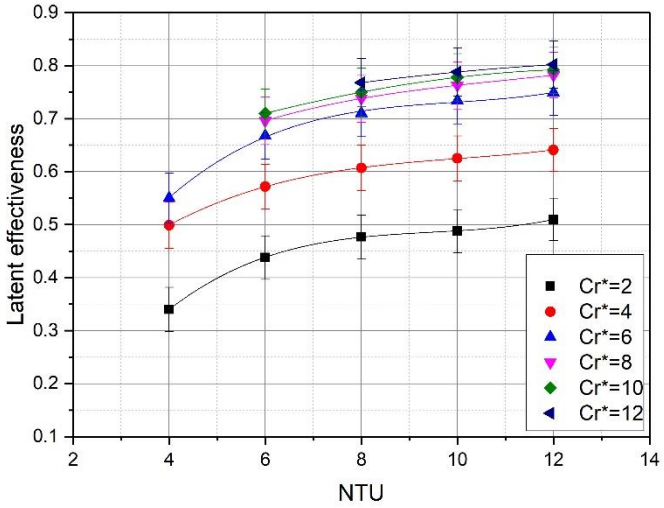

(a): *NTU* influence on latent effectiveness under different *Cr**.

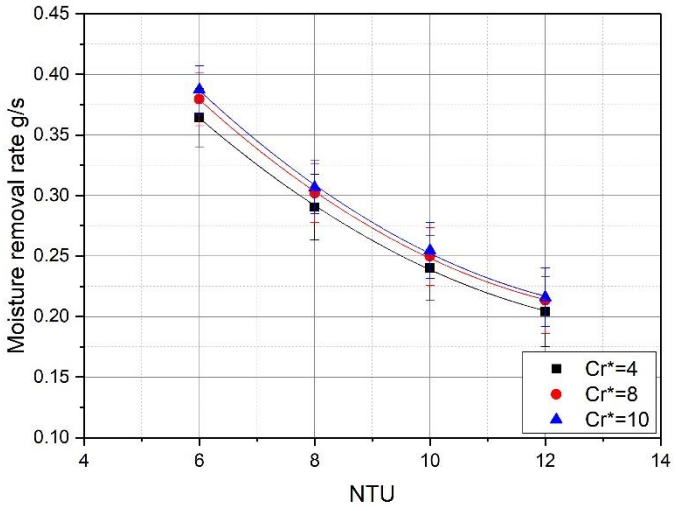

(b): Moisture removal rate variations with *NTU* under different *Cr**.

Fig. 16: (a): *NTU* influence on latent effectiveness under different *Cr**; (b): Moisture removal rate variations with *NTU* under different *Cr**.

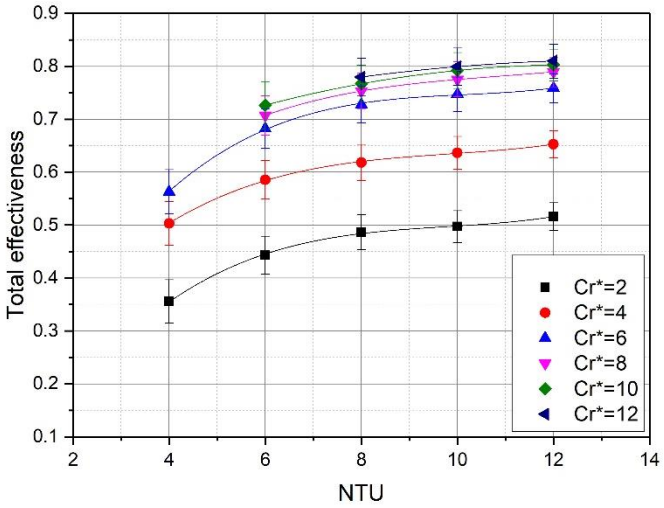

Fig. 17: *NTU* influence on total effectiveness under different *Cr**.

4. Conclusion

The experimental study of a cross flow *LAMEE* is conducted to investigate the main parameter influences by observing its air temperature fields. The tested parameters include inlet air *RH*, solution concentration and temperature, *NTU* and *Cr**. The sensible, latent, total effectiveness and air moisture removal rate are applied to assess the *LAMEE* performance. Conclusions draw from the experiment results are listed as:

- The highest air temperature is found at the corner of the air channel inlet and the desiccant solution channel outlet (exclude low *Cr** value condition), which is even higher than its inlet temperature.
- Inlet air *RH* has positive effect on the air moisture removal rate which increases 33.7% when the *RH* changes from 62% to 74%, but it has negative effect on the total effectiveness which decreases 1.7%, while the latent effectiveness almost keeps constant.
- Desiccant solution concentration has little positive impact on the *LAMEE* effectiveness while its temperature has negative influence. The latent and total effectiveness enhance with the solution concentration while its sensible effectiveness reduces. The highest total effectiveness of 0.78 is achieved with the solution concentration of 39% at 18℃, while the lowest total effectiveness of 0.672 is realised with the solution concentration of 30% at 26℃.
- Dimensionless parameters *NTU* and *Cr** have substantial positive effects on the *LAMEE* performance. However *NTU* should be not greater than 8, and *Cr** should be in the range of 2 to 6 for the tested *LAMEE*. The highest sensible, latent and total effectiveness are 0.823, 0.802 and 0.810 respectively when *Cr*=NTU*=12, while the lowest effectiveness are 0.378, 0.340 and 0.356 respectively when *Cr**=2, *NTU*=4. The recommended operating condition is *NTU*=8, *Cr**=6, and its sensible, latent and total effectiveness reach 0.758, 0.710 and 0.728 respectively.

References

[1] A.M. Omer， Energy, environment and sustainable development, Renewable and Sustainable Energy Reviews 12 (2008) 2265-2300.

[2] L. Pérez-Lombard, J. Ortiz, C. Pout， A review on buildings energy consumption information，Energy and Buildings 40 (2008) 394-398.

[3] S. Alizadeh，Performance of a solar liquid desiccant air conditioner – An experimental and theoretical approach, Solar Energy 82(2008) 563-572.

[4] K.W. Mui, L.T. Wong, L.Y. Law, An energy benchmarking model for ventilation systems of air-conditioned offices in subtropical climates, Applied Energy 84(2007) 89-98.

[5] R.H. Qi, L. Lu, H.X. Yang, Investigation on air-conditioning load profile and energy consumption of desiccant cooling system for commercial buildings in Hong Kong, Energy and Buildings 49 (2012) 509-518.

[6] G.O.G Löf, Cooling with solar energy, Congress on solar energy, Tucson Arizona, USA. 1955:171-189.

[7] A.Th. Mohammad, S.B. Mat, M.Y. Sulaiman, K. Sopian, A.A. Alabidi, Survey of hybrid liquid desiccant air conditioning systems, Renewable and Sustainable Energy Reviews 20 (2013)186–200.

[8] T. Katejanekarn, S. Kumar, Performance of a solar-regenerated liquid desiccant ventilation pre-conditioning system, Energy and Buildings 40(2008) 1252-1267.

[9] W. Kessling, E. Laevemann, C. Kapfhammer, ENERGY STORAGE FOR DESICCANT COOLING SYSTEMS COMPONENT DEVELOPMENT, Solar Energy 64(1998) 209-221.

[10] L.S. Wang, F. Xiao, X.F. Niu, D. Gao，A dynamic dehumidifier model for simulations and control of liquid desiccant hybrid air conditioning systems， Energy and Buildings 140(2017) 418-429.

[11] Y.M. Luo, H.G. Yang, L. Lu，Dynamic and microscopic simulation of the counter-current flow in a liquid desiccant dehumidifier，Applied Energy 136 (2014) 1018–1025.

[12] B. Sreelal, R. Hariharan， The Effect of Air Velocity in Liquid Desiccant Dehumidifier Based on Two Phase Flow Model Using Computational Method，International Journal of Emerging Engineering Research and Technology 2(2014) 142-152.

[13] M. Tu, C.Q. Ren, L.A. Zhang, J.W. Shao, Simulation and analysis of a novel liquid desiccant air-conditioning system, Applied Thermal Engineering 29 (2009) 2417–2425.

[14] R.S. Das, S. Jain, Simulation of potential standalone liquid desiccant cooling cycles, Energy 81 (2015) 652-661.

[15] X.H. Qu, W.J. Cai, X.X. He, D.Q. Zhai, Experimental investigations on heat and mass transfer performances of a liquid desiccant cooling and dehumidification system, Applied Energy 220 (2018) 164–175.

[16] S. Bergero, A. Chiari, On the performances of a hybrid air-conditioning system in different climatic conditions, Energy 36 (2011) 5261-5273.

[17] A.H. Abdel-Salam, G.M. Ge, G.J. Simonson, Performance analysis of a membrane liquid desiccant air-conditioning system, Energy and Buildings 62 (2013) 559–569.

[18] R. Namvar, G.M. Ge, C.J. Simons, R.W. Besant, Transient heat and moisture transfer characteristics of a liquid-to-air membrane energy exchanger (LAMEE) model verification and extrapolation, International Journal of Heat and Mass Transfer 66 (2013) 757–771.

[19] G.M. Ge, D.G. Moghaddam, A.H. Abdel-Salam, R.W. Besant, C.J. Simonson, Comparison of experimental data and a model for heat and mass transfer performance of a liquid-to-air membrane energy exchanger (LAMEE) when used for air dehumidification and salt solution regeneration, International Journal of Heat and Mass Transfer 68 (2014) 119–131.

[20] H.Y. Bai, J. Zhu, Z.W. Chen, L.N. Ma, R.Z. Wang, Performance testing of a cross-flow membrane-based liquid desiccant dehumidification system, Applied Thermal Engineering 119 (2017) 119–131.

[21] D.G. Moghaddam, R.W. Besant, C.J. Simonson, A methodology for scaling a small-scale energy exchanger performance results to a full-scale energy exchanger, International Journal of Heat and Mass Transfer 82 (2015) 555–567.

[22] M.R.H. Abdel-Salam, R.W. Besant, C.J. Simonson, Sensitivity of the performance of a flat-plate liquid-to-air membrane energy exchanger (LAMEE) to the air and solution channel widths and flow maldistribution, International Journal of Heat and Mass Transfer 84 (2015) 1082–1100.

[23] D.G. Moghaddam, R.W. Besant, C.J. Simonson, Solution-side effectiveness for a liquid-to-air membrane energy exchanger used as a dehumidifier/regenerator, Applied Energy 113 (2014) 872–882.

[24] G.M. Ge, D.G. Moghaddam, R. Namvar, C.J. Simonson, R.W. Besant, Analytical model based performance evaluation, sizing and coupling flow optimization of liquid desiccant run-around membrane energy exchanger systems, Energy and Buildings 62 (2013) 248–257.

[25] A. Vali, G.M. Ge, R.W. Besant, C.J. Simonson, Numerical modeling of fluid flow and coupled heat and mass transfer in a counter-cross-flow parallel-plate liquid-to-air membrane energy exchanger, International Journal of Heat and Mass Transfer 89 (2015) 1258–1276.

[26] S.M. Huang, M.L. Yang, X.X. Yang, Performance analysis of a quasi-counter flow parallel-plate membrane contactor used for liquid desiccant air dehumidification, Applied Thermal Engineering 63 (2014) 323-332.

[27] L.Z. Zhang, S.M. Huang, J.H. Chi, L.X. Pei, Conjugate heat and mass transfer in a hollow fiber membrane module for liquid desiccant air dehumidification: A free surface model approach, International Journal of Heat and Mass Transfer 55 (2012) 3789–3799.

[28] S.M. Huang, M.L. Yang, W.F. Zhong, Y.J. Xu, Conjugate transport phenomena in a counter flow hollow fiber membrane tube bank: Effects of the fiber-to-fiber interactions, Journal of Membrane Science 442(2013)8–17.

[29] R.J. Moffat, Contributions to the Theory of Single-Sample Uncertainty Analysis, Journal of Fluids Engineering 104 (1982) 250-258.

[30] C.J. Simonson1, R.W. Besant1, Energy wheel effectiveness: part I—development of dimensionless groups, International Journal of Heat and Mass Transfer 42 (1999) 2161-2170.

[31] ASHRAE Handbook-Fundamentals ASHRAE, Atlanta, 2005.

[32] L.A. Cisternas, E.J. Lam, An analytic correlation for the vapour pressure of aqueous and non-aqueous solutions of single and mixed electrolytes. Part II. Application and extension, Fluid Phase Equilib 62 (1–2) (1991) 11–27.

[33] F.P. Incropera, D.P. Dewitt, Fundamentals of Heat and Mass Transfer, John Wiley & Sons Inc., New York, 2002.

[34] S.M Huang, L.Z Zhang, K Tang, L.X Pei, Fluid flow and heat mass transfer in membrane parallel-plates channels used for liquid desiccant air dehumidification, International Journal of Heat and Mass Transfer 55 (2012) 2571-2580.

[35] ANSI/ASHRAE STANDARD 84-2008, Method of test for air-to-air heat/energy exchangers, American society of heating, refrigerating, and air-conditioning engineers, Atlanta.